Electronic driving mechanisms for displacive reconstruction and its lifting by hydrogen adsorption on a metallic surface alloy

N. Tsuboi, H. Okuyama, M. Nishijima, and T. Aruga*
Department of Chemistry, Graduate School of Science, Kyoto University, Kyoto 606-8502, Japan
(Received 26 March 2003; published 17 July 2003)

We investigated a bilayer Pd_3Ti surface alloy formed on Pd(100) by low-energy electron diffraction and angle-resolved photoelectron spectroscopy (ARPES). The surface alloy has $p(2\times2)$-$p4g$ symmetry and hydrogen adsorption induces transformation to $c(2\times2)$ symmetry. On the $p(2\times2)$-$p4g$ phase, the first layer is composed of a laterally distorted Pd(100) plane and the second layer consists of a $c(2\times2)$ Pd-Ti alloy. The adsorption of hydrogen removes the first layer distortion, yielding the surface with $c(2\times2)$ symmetry which is analogous to the surface of Pd_3Ti bulk alloy. The ARPES band mapping gives a rational description of the electronic driving mechanisms. The $p(2\times2)$-$p4g$ reconstruction is related to the strong polar interaction between the first-layer Pd and second-layer Ti atoms. Hydrogen-induced lifting of the reconstruction is ascribed to the repulsion among the first-layer Pd atoms due to the occupation of an in-plane antibonding state.

DOI: 10.1103/PhysRevB.68.033408 PACS number(s): 68.35.Rh, 73.20.At, 61.14.Hg

Reconstructions and structural phase transitions at surfaces have been the subject of numerous studies because they are believed to provide fundamental understanding of the collective behavior of atoms in reduced coordination environments. The driving mechanisms of the surface structural phenomena, which are often of dynamical nature, should be addressed to the electronic surface states and surface resonances.[1,2] However, there has been only a very limited amount of experimental evidence for the electronic driving mechanisms for the surface structural transitions, particularly on metal surfaces. For instance, while the reconstruction of the (100) surfaces of W and Mo is one of the best-studied topic in surface physics during the past decades[3] and extensive experimental studies have brought us a deep understanding of the structural properties of these surface in both static and dynamic aspects, we owe far much to theoretical calculations as to the electronic driving mechanism of the reconstruction except for a few fronteering photoemission experiments.[4–6]

In this Brief Report we show that the angle-resolved photoelectron spectroscopy (ARPES) band mapping, engaged with the quantitative surface crystallography by low-energy electron diffraction (LEED), gives a direct description of the electronic driving mechanism of the displacive reconstruction of ultrathin Pd_3Ti alloy film as well as the lifting of this reconstruction induced by hydrogen adsorption.

The experiments were performed in ultrahigh-vacuum chambers with base pressures below 1×10^{-10} Torr. Ti deposition was done by resistively heating a Ti wire. The pressure during the deposition was around 7×10^{-10} Torr. In the LEED experiment, intensities against primary energy (I-V) curves were recorded with a normal incident beam at an energy interval of 2 eV. The LEED simulation based on the dynamical theory was carried out using the Barbieri–Van Hove SATLEED package.[7] The phase shifts were calculated with the Barbieri–Van Hove phase shift program. The agreement between the calculated and experimental I-V curves was measured using the Pendry R factor (R_P).[8] The imaginary part of the inner potential was set to -5 eV. We calculated 14 phase shifts for the Pd(100)-$c(2\times2)$-Pd_3Ti-H surface and 10 phase shifts for the Pd(100)-$p(2\times2)$-$p4g$-Pd_3Ti surface. Photoemission band mapping was done with a high-resolution hemispherical energy analyzer mounted on a motorized two-axis goniometer and unpolarized He I radiation (21.22 eV). The light was incident in the (011) or (001) plane at an angle of 45° from the surface normal. The overall energy resolution was about 60 meV, and the acceptance angle for photoelectrons was set at 2°.

The Ti deposition at 300 K gave rise to diffuse (1×1) LEED patterns. Auger electron spectroscopy results suggest that deposited Ti atoms form three-dimensional (3D) islands. The surface was then annealed at 800–900 K to obtain a sharp $p(2\times2)$-$p4g$ pattern, which is characterized by the systematic extinction of the $(n+\frac{1}{2},0)$ and $(0,n+\frac{1}{2})$ spots [Fig. 1(a)]. The growth mechanism of a similar surface alloy in Al/Pd(100) has already studied in detail,[9] which showed that an initial Al coverage of ~2.0 was necessary in order to cover the whole surface with the $p(2\times2)$-$p4g$ surface alloy, which is composed of 1.5-monolayer (ML) Pd and 0.5-ML Al atoms, because the surface alloy formation proceeds via the stoichiometric exchange of surface Al atoms and substrate Pd atoms until 1.5 ML of Pd atoms are pushed out on the surface. For initial coverages much larger than 2.0, the LEED pattern was again degraded due possibly to the excess Al atoms in the subsurface region. We therefore estimated the optimal deposition time for the formation of the

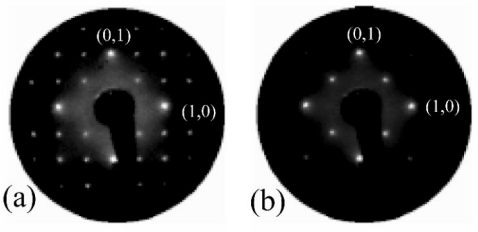

FIG. 1. LEED patterns of Ti/Pd(100) surface alloy with a primary energy of 132 eV: (a) $p(2\times2)$-$p4g$ surface at 380 K and (b) $c(2\times2)$ surface at 300 K.

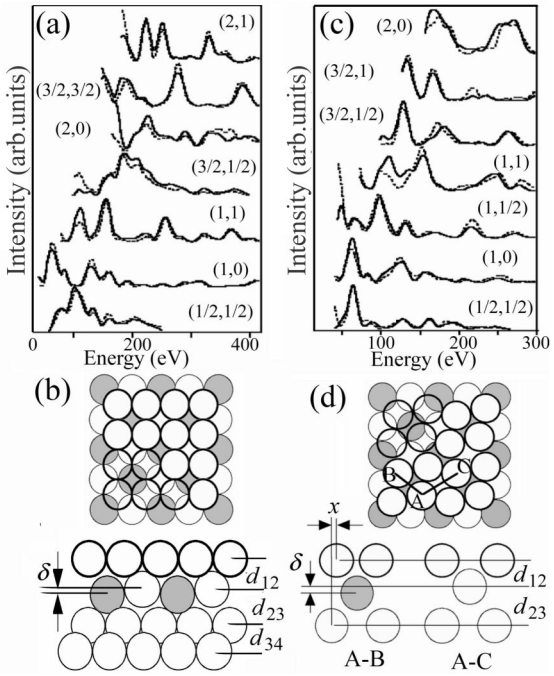

FIG. 2. Comparison between experimental (solid) and calculated (dotted) *I-V*curves for (a) the $c(2\times2)$ surface and (c) the $p(2\times2)$-$p4g$ surface. (b) Best-fit structure of Ti/Pd(100)-$c(2\times2)$-H, in top (top panel) and side view (bottom panel). (d) Best-fit structure of Ti/Pd(100)-$p(2\times2)$-$p4g$, in top (top panel) and side view (bottom panel). The white and transparent spheres are Pd and the gray ones Ti atoms.

$p(2\times2)$-$p4g$ surface by measuring the intensities of the $(1,\frac{1}{2})$ spot. When the initial Ti coverage is higher than the optimal one, the LEED pattern changes to diffuse $c(2\times2)$.

Hydrogen adsorption was done with the surface at 90–300 K, which changed the LEED patterns from $p(2\times2)$-$p4g$ to $c(2\times2)$ [Fig. 1(b)]. Thermal desorption traces of hydrogen was also monitored, which showed a characteristic line shape. With increasing initial Ti coverage, the saturation coverage of H atoms decreased from 1.0 on clean Pd(100) to 0.5 at the completion of the surface alloy with the optimal Ti coverage determined by LEED. Hydrogen was desorbed associatively from the $c(2\times2)$ surface by annealing upon 370 K, which recovered the $p(2\times2)$-$p4g$ surface.

The LEED *I-V* curves were measured at 300 K for the $c(2\times2)$ surface and at 380 K for the $p(2\times2)$-$p4g$ surface. We first determined the $c(2\times2)$ structure because of its higher symmetry. Seven beams (1,0), $(\frac{1}{2},\frac{1}{2})$, (1,1), $(\frac{3}{2},\frac{1}{2})$, (2,0), (2,1), and $(\frac{3}{2},\frac{3}{2})$ were employed in a total energy range of 1998 eV.

We prepared 35 models for the screening purpose. Ti coverages of 0.5, 1.0, and 1.5 were considered, and the outermost three layers were treated as a surface layer with the structure potentially different from those of the bulk. Hydrogen was not considered because hydrogen is a weak scatterer. A model with 0.5-ML Ti atoms in the second layer [$c(2\times2)$-*s* model: see Fig. 2(b)] yielded the best R_P of 0.20.

TABLE I. Optimized parameters for the best-fit $c(2\times2)$-H and $p(2\times2)$-$p4g$ models.

Parameters (Å)	$c(2\times2)$-H	$p(2\times2)$-$p4g$
d_{12}	1.87 ± 0.02	1.85 ± 0.04
d_{23}	1.91 ± 0.02	2.02 ± 0.04
d_{34}	1.95 ± 0.02	
δ	-0.01 ± 0.03	0.13 ± 0.03
x		0.42 ± 0.07

Other structures gave R_P from 0.43 to 0.96. The variance[8] was 0.022, which suggests that the models other than the $c(2\times2)$-*s* model can be excluded. The $c(2\times2)$-*s* model was refined with the Debye temperature taken into account. The refined structure yielded R_P of 0.157. Figure 2(a) shows the experimental *I-V* curves along with the best-fit calculated curves. The optimized values for structural parameters, the interlayer distances d_{12}, d_{23}, and d_{34}, and the intralayer buckling in the second layer, δ, are listed in Table I. The optimized Debye temperatures are 190, 260, and 310 K, respectively, for the Pd atoms in the first layer and second layer and Ti atoms in the second layer. The third layer and bulk Pd value were kept at 280 K.

The bulk Pd_3Ti alloy has a $AuCu_3$-type cubic structure, in which Pd and PdTi layers are stacked alternatively along the [100] direction. The top three layers of the H-covered $c(2\times2)$ surface may therefore be considered as a surface analog of the Pd_3Ti bulk alloy. The surface layer spacings $d_{12}=1.87\pm0.02$ Å and $d_{23}=1.91\pm0.02$ Å, are slightly contracted from that in bulk Pd (1.95 Å). While the lateral lattice constant of the surface alloy (3.89 Å) is larger than that of the bulk alloy (3.82 Å) due to the constraint by the substrate, the contracted lattice constant along the surface normal (3.78 Å) gives a unit-cell volume close to that of the bulk alloy. The Pd-Ti distances 2.69 Å [Pd(1)-Ti(2)], 2.75 Å [Pd(2)-Ti(2)], and 2.73 Å [Pd(3)-Ti(2)], where *A* (*n*) denotes the *A* atom in the *n*th layer, are comparable with or slightly longer than that in the bulk alloy, 2.70 Å .

We also tried to determine the adsorption site of hydrogen. We examined hollow, bridge, and on-top sites, which did not yield a significant difference. Thus the site of hydrogen could not be determined.

We next examined the structure of the $p(2\times2)$-$p4g$ phase. Since the H-induced transition from $p(2\times2)$-$p4g$ to $c(2\times2)$ takes place even at 90 K, we assumed that the transition is not associated with extensive mass transfer. We therefore considered the two possible structures which can be obtained by displacively reconstructing the $c(2\times2)$ structure. Both models are comprised of the topmost ''clock-reconstructed'' Pd layer, the second $c(2\times2)$-PdTi alloy layer, and the Pd(100)-(1×1) substrate. The two differ in the registry relation between the first and second layers: the center of the Pd_4 square in the first layer falls on second layer Ti in model 1 and on Pd in model 2.

We employed seven beams (1,0) $(\frac{1}{2},\frac{1}{2})$, (1,1), $(1,\frac{1}{2})$, $(\frac{3}{2},\frac{1}{2})$, $(\frac{3}{2},1)$, and (2,0), with a total range of 1542 eV. The outermost two layers were treated as the surface layers.

Model 2 yielded R_P of 0.23, which is much smaller than that for model 1 ($R_P=0.64$). We refined model 2 including the Debye temperatures and obtained $R_P=0.22$.

The calculated *I-V* curves for the best-fit structure are compared with experimental ones in Fig. 2(c). Figure 2(d) shows the refined structure, and Table I lists optimized parameters. The intralayer buckling in the second layer is significant ($\delta=0.13\pm0.03$ Å). The optimized Debye temperatures are 170, 280, and 320 K, respectively, for the Pd(1), Pd(2), and Ti(2). A remarkable characteristic of this structure is a very short Pd(1)-Ti(2) distance of 2.51 Å, which is ~7% shorter than those in the bulk alloy or in the H-stabilized $c(2\times2)$ surface alloy. The distances of Ti(2) from Pd(2) and Pd(3) are very close to the bulk value. On the other hand, the Pd(2)-Pd(3) distance (2.80 Å) is expanded by 1.8% compared with that in fcc Pd while the Pd(1)-Pd(2) distance (2.71 Å) is contracted by 1.5%. These features are very similar to the $p(2\times2)$-$p4g$ surface alloy on Al/Pd(100).[10]

The short Pd(1)-Ti(2) distance suggests that the strong bonding between these atoms drives the displacive reconstruction of the bulklike surface alloy. The H-induced transition to the $c(2\times2)$ phase is hence considered as the lifting of the displacive surface reconstruction. It might also be argued that the moderate Pd(1)-Ti(2) distance in the H-induced $c(2\times2)$ surface indicates that the strong Pd(1)-Ti(2) bonding is weakened in compensation of the H-Pd(1) bond formation. Such arguments, however, should be examined by directly studying the surface electronic structure.

In order to examine the electronic driving mechanism of these structural transitions, we carried out an ARPES experiment to determine the band dispersion along the $\bar{\Gamma}$-$\bar{X}$ and $\bar{\Gamma}$-$\bar{M}$ directions, where $\bar{X}$ and $\bar{M}$ denote the symmetry points in the $p(1\times1)$ surface Brillouin zone. We observed significant changes of surface electronic structure around the $\bar{M}$ point, where several surface resonances were predicted for clean Pd(100) by theoretical calculations.[11–13]

Figure 3(a) shows the band mapping results for Pd(100). The photoemission intensity is normalized to the Fermi-Dirac function in order to reveal the bands near and above E_F.[14] For clean fcc(100) surfaces, the well-known Tamm state ($\bar{M}_3$) is located near the bottom of the projected bulk band gap at $\bar{M}$. In the case of Pd, the lower edge of the projected band gap is slightly above E_F and the $\bar{M}_3$ state is located at 0.2–0.7 eV above E_F.[11–13] Theoretical calculations for the (100) surfaces of group-10 elements [Ni (Ref. 15), Pd (Ref. 11–13), Pt (Ref. 16)] predict the presence of a surface resonance band along $\bar{\Gamma}$-$\bar{M}$ that is strongly localized to the topmost layer and leads to the $\bar{M}_3$ surface state above E_F. Band (1) in Fig. 3(a) is in good agreement with this surface resonance band. In Fig. 3(a), an intense photoemission is observed at E_F at $\bar{M}$. This is assigned to the emission from the bulk Z_2 band, which has a negligible dispersion along X-W and hence gives rise to high projected density of states at $\bar{M}$.

The theoretical calculations also predict another surface resonance state ($\bar{M}_1$) just below E_F. The dispersion and energy of band (2) in Fig. 3(a) is in good agreement with this surface resonance band. The band seen at a binding energy of ~1.2 eV at $\bar{M}$ has no counterpart in many of the predicted surface resonances. As shown in Fig. 3(b), the hydrogen adsorption on Pd(100) gives rise to the downward shift by ~0.2 eV of this state. Therefore the state at 1.2 eV may be assigned to surface resonances, which should have d_{xz} and d_{yz} characters. Negligible changes are observed in surface resonance bands (1) and (2) upon H adsorption. The *ab initio* band calculation for H/Pd(001) (Ref. 13) indicates that the unoccupied $\bar{M}_3$ surface state should be strongly influenced by H adsorption. The calculations also predict an $\bar{M}_4$ surface resonance at ~4 eV, which was not observed in the present work due possibly to a small photoionization cross section under the condition employed.

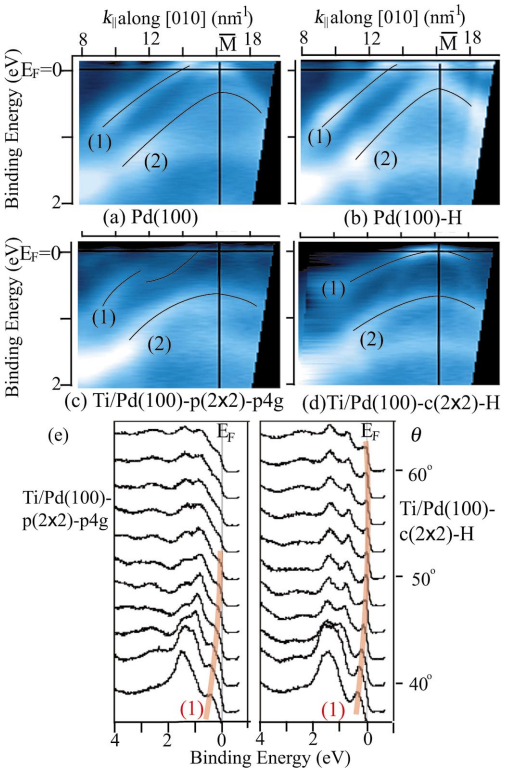

FIG. 3. (Color) Experimental surface band dispersion along $\bar{\Gamma}\bar{M}$: (a) clean Pd(100) surface, (b) Pd(100)-H surface, (c) Ti/Pd(100)-$p(2\times2)$-$p4g$ surface, and (d) Ti/Pd(100)-$c(2\times2)$-H surface. The black lines are shown as guides. (e) ARPE spectra for $p(2\times2)$-$p4g$ and $c(2\times2)$-H surfaces along $\bar{\Gamma}\bar{M}$. Here $\bar{M}$ corresponds to 51.8° at E_F and $k_\parallel=\sqrt{(2m_e/\hbar^2)E_{kin}}\sin\theta$, where E_{kin} is the kinetic energy of the detected electron.

Figure 3(c) shows the band mapping for the $p(2\times2)$-$p4g$ surface alloy. A significant change as compared with the clean surface is observed in the energy position of the $\bar{M}_1$ state [band (2)], which is shifted downward by 0.4 eV. The $\bar{M}_1$ state has a $d_{3z^2-r^2}$ character. As schematically depicted in Fig. 4(a), the $d_{3z^2-r^2}$ orbital has a π-bonding character with respect to the Pd(1)-Ti(2) bond at around the $\bar{M}$ point. For the chemical bond between Pd (with mostly occupied *d* states) and Ti (with mostly empty *d* states), the

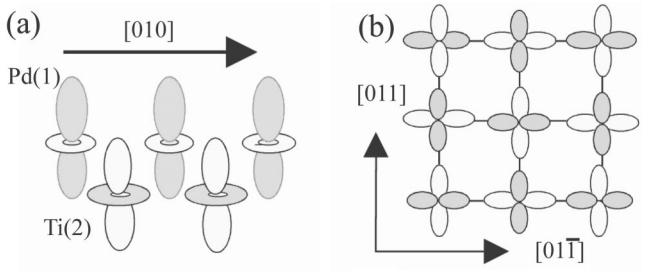

FIG. 4. (a)Schematic representation of the interaction between the first-layer Pd and second-layer Ti $d_{3z^2-r^2}$ orbitals at the $\bar{M}$ point. (b) Schematic representation of the interaction of the first layer d_{xy} orbitals at the $\bar{M}$ point. The different colors refer to the different sign of the wave function.

bonding state should inherit a wave function character mainly from the Pd *d* state and be shifted to a higher binding energy as compared with the corresponding state in pure Pd. This is in good agreement with the observed shift of the $\bar{M}_1$ state upon the formation of the surface alloy. The formation of the strong Pd(1)-Ti(2) bond is in good agreement with the unusually short Pd(1)-Ti(2) bond length as determined by LEED.

Another noticeable but less significant change upon the surface alloy formation is seen in the dispersion of band (1), which appears to be split into two bands dispersing in parallel. This may be due to the lowering of the translational symmetry. The $\bar{M}_3$ state, however, is still well above E_F.

The hydrogen adsorption on the surface alloy also induces a significant change in the surface electronic structure. Upon the hydrogen adsorption, band (1) shifts downward and the $\bar{M}_3$ state reaches at $E \sim E_F$ [Fig. 3(d)]. The change is also clearly seen in the raw ARPE spectra shown in Fig. 3(e). The $\bar{M}_3$ state has a pure d_{xy} character localized in the (100) atomic plane and is fully decoupled from the state in the adjacent layer because of symmetry.[17,18] (Here *x*, *y*, and *z* refer to the bulk cubic directions with *z* perpendicular to the surface.) This change is very important, since the $\bar{M}_3$ has a strong antibonding character with respect to the in-plane chemical bond between Pd atoms [Fig. 4(b)]. The antibonding character is expected both for the nearest-neighbor pairs along [011] and for the next-nearest-neighbor pairs along [010]. In the $p(2\times2)$-$p4g$ structure, the distance (3.05 Å) between two adjacent Pd(1) atoms along [010] coordinated to the same Ti(2) atom is well within the direct bonding interaction, resulting in the effectively fivefold in-plane coordination. The H-induced occupation of the antibonding $\bar{M}_3$ state should tends to decrease the in-plane coordination number, which can explain the H-induced destabilization of the $p(2\times2)$-$p4g$ reconstruction. On the other hand, the $\bar{M}_1$ state exhibits negligible shift upon the H adsorption, which suggests that the Pd(1)-Ti(2) bonding is maintained in the H-covered $c(2\times2)$ surface. The lifting of the displacive reconstruction is therefore understood as resulting from the competition between the two opposing effects, i.e., the Pd(1)-Ti(2) attraction and the in-plane repulsion among Pd(1) atoms.

In summary we have shown that the electronic driving mechanisms of the rather complexed structural changes in the metallic surface system can be discussed quantitatively. We observed a $p(2\times2)$-$p4g$ reconstruction on the Ti/Pd(100) surface alloy and determined its structure. The hydrogen adsorption lifts the displacive reconstruction and forces the surface to a bulk-Pd_3Ti-like $c(2\times2)$ structure. Examination of both the atomic and electronic structure suggests that the $p(2\times2)$-$p4g$ reconstruction is driven by the strong polar bonding between Pd(1) and Ti(2) atoms. This bond is maintained even after the displacive reconstruction is lifted by the hydrogen adsorption. Hydrogen-induced lifting of the reconstruction is instead addressed to the occupation of the $\bar{M}_3$ surface resonance state with in-plane antibonding character.

We thank Dr. Seigi Mizuno for his helpful suggestions.

*Electronic address: aruga@kuchem.kyoto-u.ac.jp

[1] *Electronic Surface States and Interface States on Metallic System*, edited by E. Bertel and M. Donath (World Scientific, Singapore, 1995).
[2] P. Sandl and E. Bertel, Surf. Sci. Lett. **302**, L325 (1994).
[3] J. Jupille and D.A. King, in *The Chemical Physics of Solid Surfaces*, edited by D.A. King and D.P. Woodruff (Springer-Verlag, Amsterdam, 1994), p. 35.
[4] K.E. Smith and S.D. Kevan, Phys. Rev. B **43**, 3986 (1991).
[5] G.S. Elliott, K.E. Smith, and S.D. Kevan, Phys. Rev. B **44**, 10 826 (1991).
[6] J.W. Chung, K.S. Shin, D.H. Baek, C.Y. Kim, H.W. Kim, S.K. Lee, C.Y. Park, S.C. Hong, T. Kinoshita, M. Watanabe, A. Kakizaki, and T. Ishii, Phys. Rev. Lett. **69**, 2228 (1992).
[7] A. Barbieri and M.A. Van Hove, Symmetrized Automated Tensor LEED package, available from M. A. Van Hove.
[8] J.B. Pendry, J. Phys. C **13**, 937 (1980).
[9] K. Kishi, A. Oka, N. Takagi, M. Nishijima, and T. Aruga, Surf. Sci. **460**, 264 (2000).
[10] H. Onishi, H. Sakama, T. Aruga, A. Kawazu, and Y. Iwasawa, Surf. Sci. **444**, 7 (2000).
[11] J.G. Gay, J.R. Smith, F.J. Arlinghaus, and T.W. Capehart, Phys. Rev. B **23**, 1559 (1981).
[12] M. Heinrichsmeier, A. Fleszar, W. Hanke, and A.G. Eguiluz, Phys. Rev. B **57**, 14 974 (1998).
[13] W. Dong, V. Ledentu, Ph. Sautet, A. Eichler, and J. Hafner, Surf. Sci. **411**, 123 (1998).
[14] T. Greber, T.J. Kreutz, and J. Osterwalder, Phys. Rev. Lett. **79**, 4465 (1997).
[15] O. Jepsen, J. Madsen, and O.K. Andersen, Phys. Rev. B **26**, 2790 (1982).
[16] Ding-sheng Wang, A.J. Freeman, and H. Krakauer, Phys. Rev. B **29**, 1665 (1984).
[17] G.P. Alldredge and L. Kleinman, Phys. Rev. B **10**, 559 (1974).
[18] D.W. Bullet, J. Phys. C **14**, 4521 (1981).